Atomic-Scale Design of Iron Fischer-Tropsch Catalysts: A Combined Computational Chemistry, Experimental, and Microkinetic Modeling Approach

3rd Annual Report

Award Number: DE-FC26-03NT41966

Professor Manos Mavrikakis,
Professor James A. Dumesic,
Rahul P. Nabar
Department of Chemical and Biological Engineering
University of Wisconsin - Madison
Madison, WI 53706

Professor Calvin H. Bartholomew,
Dr. Hu Zou,
Uchenna Paul
Department of Chemical Engineering
Brigham Young University
Provo, UT 84602

February 2, 2007

Disclaimer

Abstract

Work continued on the development of a microkinetic model of Fischer-Tropsch synthesis (FTS) on supported and unsupported Fe catalysts. The following aspects of the FT mechanism on unsupported iron catalysts were investigated on during this third year: (1) the collection of rate data in a Berty CSTR reactor based on sequential design of experiments; (2) CO adsorption and CO-TPD for obtaining the heat of adsorption of CO on polycrystalline iron; and (3) isothermal hydrogenation (IH) after Fischer Tropsch reaction to identify and quantify surface carbonaceous species. Rates of C_{2+} formation on unsupported iron catalysts at 220ºC and 20 atm correlated well to a Langmuir-Hinshelwood type expression, derived assuming carbon hydrogenation to CH and OH recombination to water to be rate-determining steps. From desorption of molecularly adsorbed CO at different temperatures the heat of adsorption of CO on polycrystalline iron was determined to be 100 kJ/mol. Amounts and types of carbonaceous species formed after FT reaction for 5~10 minutes at 150, 175, 200 and 285ºC vary significantly with temperature.

Mr. Brian Critchfield completed his M.S. thesis work on a statistically designed study of the kinetics of FTS on 20% Fe/alumina. Preparation of a paper describing this work is in progress.

Results of these studies were reported at the Annual Meeting of the Western States Catalysis and at the San Francisco AIChE meeting.

In the coming period, studies will focus on quantitative determination of the rates of kinetically-relevant elementary steps on unsupported Fe catalysts with/without K and Pt promoters by SSITKA method. This study will help us to (1) understand effects of promoter and support on elementary kinetic parameters and (2) build a microkinetics model for FTS on iron.

Calculations using periodic, self-consistent Density Functional Theory (DFT) methods were performed on models of defected Fe surfaces, most significantly the stepped Fe(211) surface. Binding Energies (BE's), preferred adsorption sites and geometries of all the FTS relevant stable species and intermediates were evaluated. Each elementary step of our reaction model was fully characterized with respect to its thermochemistry and comparisons between the stepped Fe(211) facet and the most-stable Fe(110) facet were established. In most cases the BE's on Fe(211) reflected the trends observed earlier on Fe(110), yet there were significant variations imposed on the underlying trends. Vibrational frequencies were evaluated for the preferred adsorption configurations of each species with the aim of evaluating the entropy-changes and pre-exponential factors for each elementary step. Kinetic studies were performed for the early steps of FTS (up to CH_4 formation) and CO dissociation. This involved evaluation of the Minimum Energy Pathway (MEP) and activation energy barrier for the steps involved. We concluded that Fe(211) would allow for far more facile CO dissociation in comparison to other Fe catalysts studied so far, but the other FTS steps studied remained mostly unchanged.

Table of Contents

Introduction

A. Background

Fischer-Tropsch Synthesis (FTS) has been used commercially for more than 70 years in the conversion of syngas (H_2/CO), derived from coal or natural gas, into liquid hydrocarbons [1,2]. Its application to production of liquid fuels from natural gas (GTL) is expanding into a large world-wide industry, while its application to conversion of syngas from renewable biomass is being researched. Gasoline and diesel fuels produced from FT synthesis are premium products of low aromaticity and zero sulfur content. Although FTS is in some respects a "mature technology", substantial improvements have been realized during the past three decades in catalyst, reactor, and process technologies as a result of intensive research. Moreover, improvements could yet be realized in catalyst and reactor design through a deeper fundamental understanding of the reaction mechanism and catalyst activity-structure relationships. Combined application of modern surface science and computational chemistry tools is a powerful methodology for realizing deeper understanding required for improving catalyst design.

Almost 80 years ago, Fischer and Tropsch postulated that CO hydrogenation takes place on bulk carbides of Co and Fe. Over the decades a consensus has emerged that FTS is a polymerization process involving addition of a CH_x (x = 0-2) monomer to a growing hydrocarbon chain. The formation of the surface CH_x is proposed to occur via adsorption of CO on a metal site and dissociation of CO to a surface carbon atom, i.e. a surface carbide (C(ad)), followed by stepwise addition of H atoms to produce methylidyne (CH(ad)), methylene (CH_2(ad)) methyl (CH_3(ad)) species. However, there is little quantitative information regarding the potential energies of these intermediates or the kinetic parameters for these and the subsequent elementary steps producing hydrocarbons. Moreover, there is little consensus regarding the mechanisms of C-C coupling, i.e. which of the CH_x species are involved in this important step for either Co or Fe catalysts.

Both Co and Fe catalysts have been used commercially for FTS. Fe catalysts were used for 55 years at Sasol for conversion of coal to fuels and chemicals because of their low cost and ability to process coal syngas having low H_2/CO ratios as a result of their high activities for the water gas shift reaction. For the same reason Fe catalysts are favored for production of fuels from biomass. Since Co catalysts are more productive and stable than Fe catalysts, they are presently favored in GTL processes; nevertheless, the low cost and low methane selectivity of Fe catalysts make them an attractive option, especially if more productive, stable, supported Fe catalysts can be developed. A

microkinetics model for Fe FTS could enable the needed improvements in design. There are no previously reported microkinetic studies of FTS on Fe.

This report describes progress made during the second year of a three-year DOE-sponsored project for advanced design of supported iron Fischer-Tropsch catalysts through development of a microkinetics model for FTS based on theoretical computations and mechanistic experiments. The BYU catalysis research team is assisting the computations team at U. Wisconsin through study and search of literature addressing FTS kinetics and mechanisms, experimental mechanistic studies of elementary reactions, and the development of rate data for alumina supported iron FTS catalysts.

B. Work Statement

1. Objectives

The principal objective of this work is to develop and validate a detailed microkinetics submodel describing the rates of the important elementary steps that occur during FTS on the surface of an iron catalyst, which incorporates the effects of K and Pt promoters, support and of surface and subsurface carbon species on the these important elementary steps.

2. Scope

This microkinetics submodel will enable prediction of catalyst activity and hydrocarbon selectivities over a range of temperatures, pressures, and H_2/CO ratio and as a function of promoter type, and of surface carbon coverage. It will address the molecular principles that govern the relative rates of chain growth versus termination on iron FT catalysts, thereby providing a basis for maximizing desirable products (e.g. olefins, diesel liquids and waxes) while minimizing formation of undesirable products such as methane, LPG, and alcohols.

3. Tasks

To accomplish the above objectives, the proposed research has been divided into the following specific tasks to be accomplished over a period of 36 months:

Task 1: Search literature and incorporate available kinetic parameters into a microkinetics model for FT surface reactions on iron; determine consistency of available data and needs for obtaining additional parameters—this will be an ongoing task. **(BYU and UW)**

Task 2: Measure kinetic parameters for key elementary steps including CO and H_2 adsorptions/desorptions, CO dissociation, C hydrogenation, olefin adsorption on unpromoted Fe catalysts and Fe catalysts promoted with K_2O and/or Pt. Catalysts will be prepared using co-precipitation and non-aqueous, evaporative deposition

methods and will be characterized by H_2 and CO adsorptions, XRD, TPR, TEM, and BET methods. Studies of elementary steps will be conducted at high pressure conditions using TPD and temperature-programmed reaction spectroscopies combined with isotopic tracer studies. **(BYU)**

Task 3: Use DFT Calculations to determine reaction thermochemistry and kinetics for key elementary steps in Tasks 1 and 2, including propagation and termination steps and steps involving reactive intermediates such as hydrogenation of CH_2. Investigate effects of surface/subsurface O and C, at various concentrations, on the reactivity of Fe surfaces. Determine effects of promoter type and concentration, coverage of surface/subsurface carbon species, and surface defects on the kinetic/thermodynamic parameters for key steps. **(UW)**

Task 4: Obtain a statistical set of rate and selectivity data on $Fe/K_2O/Pt/Al_2O_3$ catalysts over a relevant range of reaction temperatures, reactant compositions, and H_2/CO ratios at commercially relevant pressures and use these data to validate the microkinetics model**.** Data will be obtained using a Berty CSTR reactor system. **(BYU and UW)**

Task 5: Build collaborative relationships with other research groups and companies and develop proposals for funding the continuation of the proposed work and its incorporation into a comprehensive catalyst particle/reactor/process model. **(BYU and UW)**

4. Deliverables

1. A microkinetics submodel that will enable prediction of catalyst activity and hydrocarbon selectivities over a range of temperatures, pressures, H_2/CO ratio, and as a function of promoter type, and of surface carbon coverage and address the molecular principles that govern the relative rates of chain growth versus termination on Fe FT catalysts, thereby providing a basis for maximizing desirable products.
2. First-Principles DFT calculations of binding energies, reaction barriers, and pre-exponential factor estimates for key elementary steps in the FTS mechanism.
3. Experimental values of kinetic parameters for key elementary steps including CO and H_2 adsorptions/desorptions, CO dissociation, C hydrogenation, and olefin adsorption on unpromoted and promoted $Fe/K_2O/Pt$ under high pressure conditions using TPD and temperature-programmed reaction spectroscopies combined with isotopic tracer studies.

4. A statistical set of rate and selectivity data on $Fe/K_2O/Pt$ catalysts over a relevant range of reaction temperatures, reactant compositions, and H_2/CO ratios that can be used to validate mechanistic models.

Executive Summary

The principal objective of this research is to develop and validate a detailed microkinetics model which describes the rates of the important elementary steps that occur on the surface of an iron catalyst during FTS. The model will incorporate the effects of K and Pt promoters, support, and surface carbon species on the important elementary steps.

Efforts during this third year focused on (1) searching/summarizing published FTS mechanistic and kinetic studies of FTS reactions on iron catalysts; (2) investigation of CO adsorption/desorption on unsupported iron catalysts to obtain CO heat of adsorption on polycrystalline iron; (3) investigation of isothermal hydrogenation of surface carbonaceous species formed in FT reaction on unsupported iron catalysts; (4) sequential design of experiments, collection of rate data in a Berty CSTR reactor, and nonlinear-regression analysis to obtain kinetic parameters on unsupported iron catalysts.

CO adsorbs both molecularly and dissociatively at room temperature on polycrystalline iron. On unsupported polycrystalline iron catalysts the two forms of adsorbed CO desorb at about 117 and 579ºC, respectively. The ratio of these two types change with adsorption temperatures. The amount of molecularly-adsorbed CO decreases while the amount of dissociatively-adsorbed CO increases with increasing adsorption temperature. Thus, CO dissociation is facilitated at higher adsorption temperature. Only dissociatively-adsorbed CO is observed above 150ºC. The heat of adsorption of CO on polycrystalline Fe was found to be about 100 kJ/mol.

Carbonaceous species formed during FT reaction for only 5~10 minutes on unsupported iron catalysts at various temperatures, i.e., 150, 175, 200 and 285ºC, were initially hydrogenated at the same temperature as FT reaction. Isothermal hydrogenation at 285ºC yielded comparatively larger amounts of carbonaceous species relative to isothermal hydrogenations at 150ºC and 175ºC. This observation indicates the formation of multi-layer carbonaceous species on the surface at 285ºC. To quantify the surface carbonaceous species, three models based on different mechanisms of hydrogenation were proposed and tested against the data. However, none of the mechanisms adequately describes the data, and it is apparent that other factors, including the flow hydrodynamics must be considered. This has led to a redesign of our TPD reactor.

A set of statistically-designed experiments was undertaken to collect steady-state rate data in a Berty CSTR reactor at 220ºC and 20 atm on unsupported iron catalysts. The data were fitted to various rate expressions using nonlinear-regression analysis to obtain kinetic parameters. Rates of C_{2+} formation correlated well to a Langmuir-Hinshelwood

type expression derived assuming two steps, carbon hydrogenation to CH and OH recombination to water as the rate-determining steps.

In the coming period, studies will focus on quantitative determination of the rates of kinetically-relevant elementary steps on Fe catalysts with/without K and Pt promoters and at various levels of Al_2O_3 support by SSITKA method, providing a database for understanding (1) effects of promoter and support on elementary kinetic parameters and (2) for validation of computational models that incorporate effects of surface structure and promoters. Kinetic parameters will be incorporated into a microkinetics model, enabling prediction of rate without invoking assumptions, e.g. of a rate-determining step or a most-abundant surface intermediate.

On the theoretical side, our work in the third year of the project focused on conducting a detailed study for FTS on a defected Fe surface. The Fe(211) system was chosen as the best model, which was viable computationally as well as gave a good representation of the defect sites present in catalytic nanoparticles. Using state-of-the-art Density Functional Theory (DFT) methods our FTS reaction-model (comprising of 32 elementary steps involving 19 species) was fully characterized with respect to its thermochemistry which involved evaluation of the Binding Energies (BE's), preferred adsorption sites and geometries of all the component stable species and intermediates. A comparison with the previously studied Fe(110) surface indicated that in most cases the trends in BE on Fe(211) paralleled those on Fe(110), yet there were significant variations imposed on this underlying trend. An evaluation of the vibrational frequencies for each species in its preferred adsorption configuration was also performed which serves as an extension of the database of vibrational frequencies previously established for Fe(110), Fe_C(110) and Fe^{Pt}(110). In particular, this provides a useful connection with experimental vibrational frequency work (e.g.: IRAS, HREELS, etc) while allowing us to compute entropy-changes and pre-exponential factors for each elementary reaction step. Finally, we performed a kinetic analysis for the early FTS steps (up to CH_4 formation) and CO dissociation; this involved calculating the Minimum Energy Pathways (MEPs) and activation energy barrier for the steps involved using the Climbing Image Nudged Elastic Band (CI-NEB) method, a state-of-the-art iterative method. CO dissociation had been a particularly difficult (high barrier) step on all the Fe systems studied so far but we found that Fe(211) offered a facile alternative for CO dissociation; the other FTS steps studied were not significantly affected. Overall, significant progress was achieved in characterizing the Fe(211) facet, but we must await completion of a kinetic analysis for the remaining steps (involving the C_2 species) before we can draw quantitative conclusions regarding the importance of various FTS pathways on Fe(110) vs Fe(211).

Results and Discussion

A. Preparation of 99 wt% Fe/1 wt % Al_2O_3/monolith (99FeAl-monolith) Catalyst and Kinetic study

1. Preparation of unsupported catalysts.

Preparation of the unsupported iron catalysts on a monolith support was conducted by impregnation from the iron nitrate melt of an acid-treated monolith surface. Two 400 mesh, 2 inch diameter and 1 inch length monoliths and two 300 mesh, 2 inch diameter, 0.5 inch length monoliths were cleaned in a 20 volume % nitric acid 80 volume % HPLC grade water solution overnight at 60°C and rinsed with HPLC grade water. A typical impregnation procedure was as follows. $Fe(NO_3)_3 \cdot 9H_2O$ (147g) and $Al(NO_3)_3 \cdot 9H_2O$ (1.5 g) were melted in a beaker heated in a water bath at 70ºC. Monoliths were dipped in the melt for approximately 1 minute, then shaken and blown out with ultra high purity helium. The samples were dried overnight at 60°C and calcined at 300°C for approximately 6 h, initially heating at a rate of 1°C/min. This procedure was repeated once. The wt% of elemental Fe on the monolith is summarized in Table 1.

Table 1. Summary of weight percentage.

Sample	Fe_2O_3 wt %	Fe wt %
1	22.59	15.81
2	22.89	16.02
3	21.73	15.21
4	21.91	15.34

TPR was conducted in the TGA system by flowing 180 mL/min of N_2 and 20 mL/min of H_2 over the sample. The temperature was linearly increased from 25ºC to 800ºC at 5ºC/min. The TPR spectrum is shown in Fig 1. Peaks having maxima at 340°C and 475°C are assigned to the reduction of Fe_2O_3 to Fe_3O_4 and the reduction of Fe_3O_4 to Fe metal, respectively. These two peaks are similar to those observed previously for a 99FeAl powder catalyst, indicating that these two catalysts are comparable. The 99FeAl-monolith catalysts were used in a steady-state kinetic study.

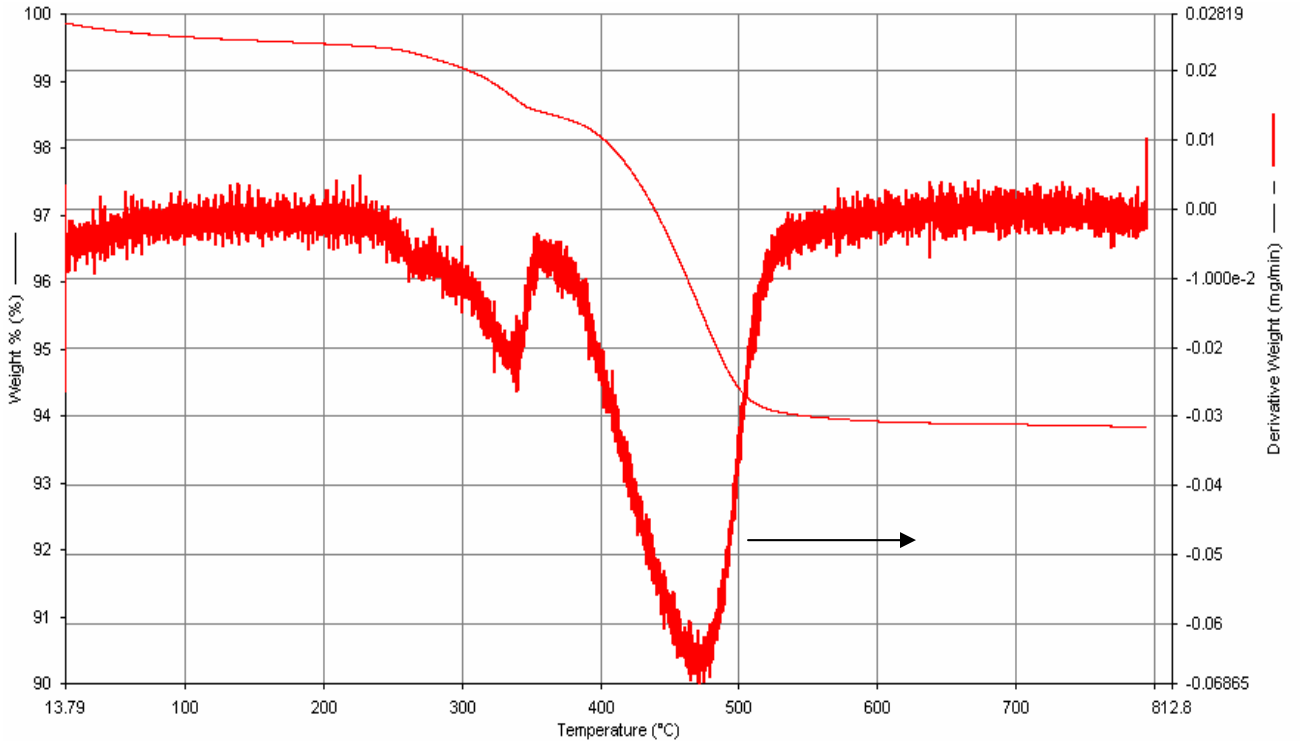

Figure 1. Temperature-programmed reduction spectrum for 99FeAl-monolith catalyst**.**

2. Kinetic study of unsupported catalysts.

A kinetic study of the unsupported catalysts was carried out our Berty CSTR-gas, fixed-bed catalysts reactor. Experimental conditions were chosen using sequential design of experiments based on a D-optimal criterion in order to generate increasingly greater statistical confidence on the regressed kinetic parameters with each step in the sequence. An L-M non-linear regression algorithm in polymath software was used to obtain values of the kinetic constants, calculation of confidence intervals and correlation coefficients.

The catalyst was reduced in 20% H_2 and 80% He (total gas flow rate of 200 mL/min) using the following reduction profile: 1) heat from room temperature to 400ºC at 0.5ºC/min; 2) hold at 400ºC for 36 h; 3) cool to 380ºC at 0.5ºC/min; 4) hold at 380ºC and purge with H_2 in He for 24 h; 5) after reducing the catalyst, the reactor was cooled to 220ºC.

Scoping runs were done at 220ºC and a total pressure of 20 atm using a 2^n factorial experimental design with center point design based on two parameters – outlet partial pressures of CO (P_{CO}) and H_2 (P_{H2}) while blocking temperature. These 5 points provided the starting data for the sequential design of experiment using the rate expression

$$-r_{C2+} = \frac{AP_{CO}^{2/3}P_{H2}^{5/6}}{(1+BP_{CO}^{2/3}P_{H2}^{1/3})^2} \qquad (1)$$

Reactor pressure was held constant at 20 atm while partial pressures of CO and H_2 were varied stepwise according to the results of the previous step in the sequential design. The first run was conducted at a standard condition that was repeated after a few runs to check for catalyst deactivation.

Figures 2 and 3 show typical plots of rate and conversion of CO as a function of time for Run #3 (see the Table 2 for the run conditions). Table 2 is a summary of run conditions and results for 9 runs; Table 3 lists the values of the regressed constants and their confidence intervals as a function of run number; and Figure 4 is a graph of the regressed kinetic parameters at 220ºC as a function of run. Figure 5 is a parity plot of calculated rate of C_{2+} versus observed rate of C_{2+}.

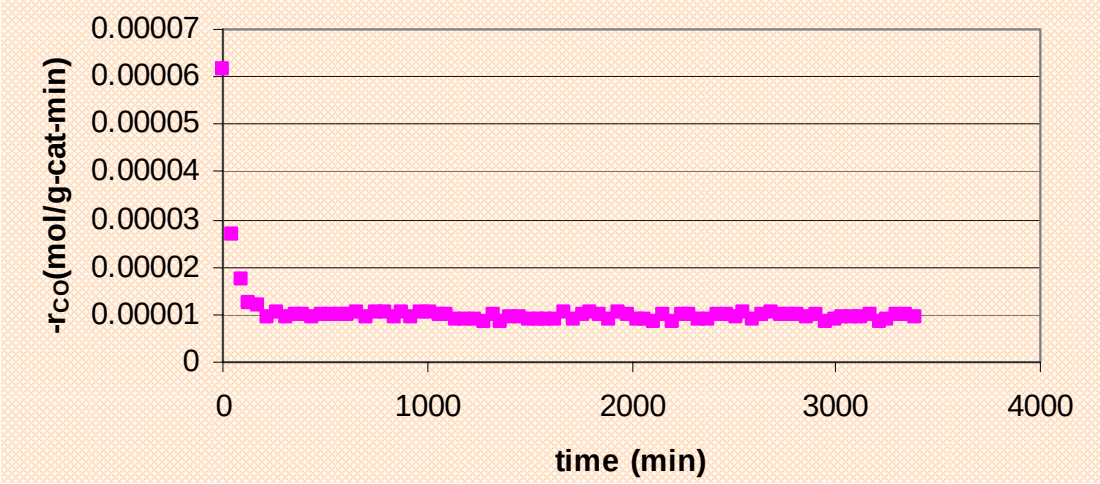

Figure 2. Rate of CO versus time for Run #3 (P_{CO} = 3.263 atm and P_{H2} = 2.351 atm).

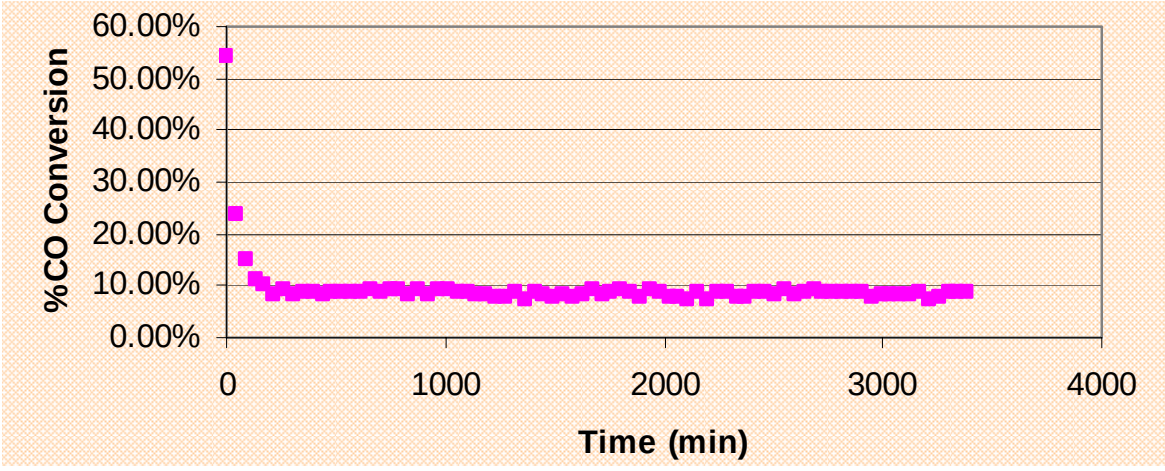

Figure 3. Conversion of CO versus time for run #3 (P_{CO} = 3.263 atm and P_{H2} = 2.351 atm)

Table 2. Summary of run conditions and results

Run #	Inlet vol. flow rate of He + Ar @ STP (mL/min)	Inlet vol. flow rate of H_2 @ STP (mL/min)	Inlet vol. flow rate of CO @ STP (mL/min)	% Conv. of CO	Outlet Partial Pressure of H_2 (atm)	Outlet Partial Pressure of CO (atm)	Rate of CO (mol/g-cat min) x 10^6	Rate of C_{2+} (mol/g-cat min) x 10^6	$\%CH_4$ Selec.	$\%CO_2$ Selec.
1	60.231	130.2	59.828	17.44	6.426	3.037	93.1421	57.01	15.057	23.72
2	108.202	130.2	11.157	83.39	6.194	0.115	78.7125	36.43	39.0	14.72
3	138.189	52.4	59.820	8.36	2.351	3.263	42.5035	18.60	9.64	46.61
4	186.484	52.6	11.511	48.92	2.045	0.351	47.522	26.72	20.38	23.39
5	124.738	90.2	35.662	22.12	3.964	1.69	66.9659	40.26	16.33	23.55
6	Standard Condition (Same as run #1) to check for catalyst deactivation									
7	22.703	44.352	25.886	26.76	5.365	3.407	58.1041	38.2	10.96	23.3
8	35.845	57.579	27.843	26.04	5.382	2.747	60.9819	39.52	13.19	22.01
9	43.462	71.13	29.278	25.59	5.739	2.409	62.7296	39.65	15.85	20.94

Table 3. Values of regressed constants and confidence intervals as a function of run number

Regression #	A mol/(g-cat x atm^1.5)		B atm^-1		Number of Runs
	Regressed Value	Confidence Interval	Regressed Value	Confidence Interval	
1	5.13E-05	5.50E-05	0.5799117	0.5566209	5
2	5.32E-05	4.37E-05	0.6127011	0.4217881	6
3	5.41E-05	3.45E-09	0.6318204	3.27E-05	7
4	5.48E-05	2.94E-07	0.6502908	2.78E-03	8

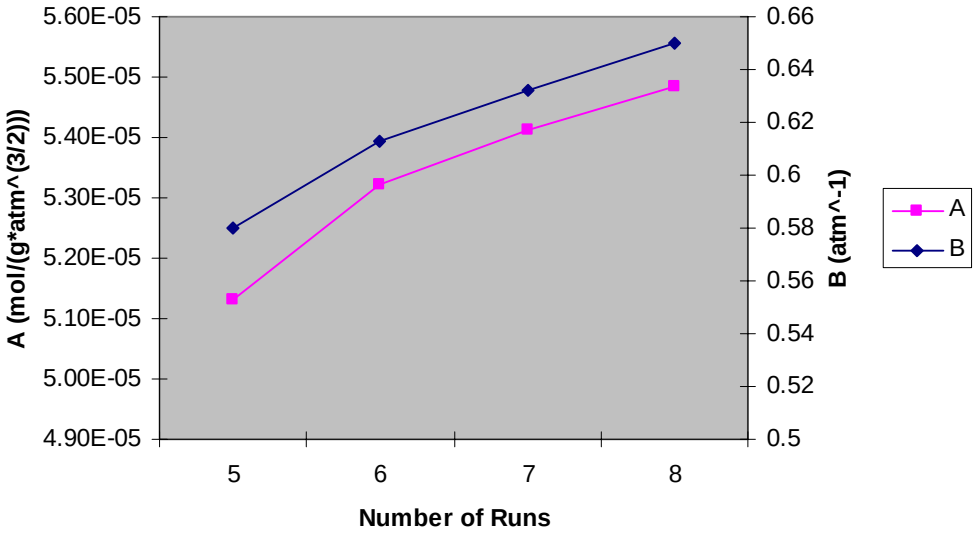

Figure 4. Graph of regressed kinetic constants as a function of number of experimental runs.

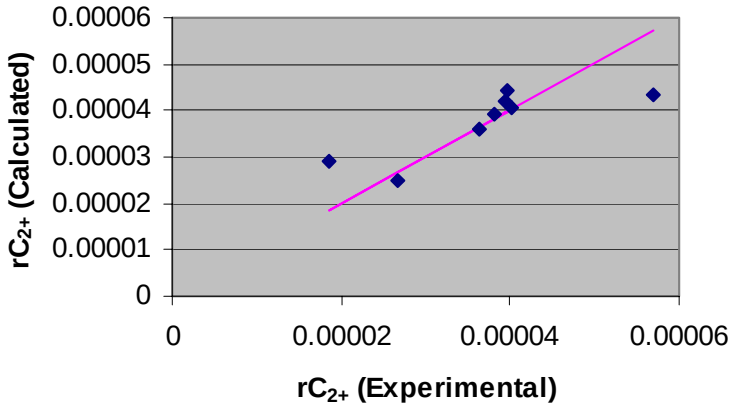

Figure 5. Parity plot of calculated rate of C_{2+} vs observed rate of C_{2+}.

It is evident from Figures 2 and 3 that steady state values of rate and conversion are reached within about 300 minutes (5 hours) after reaction conditions were changed; moreover, rate and conversion were steady over the next 45 hours. Generally, data were collected for much more than 5 hours after each change of conditions to ensure steady-state had been reached and as a check on catalyst stability. A repeat run (Run #6) at standard condition also served as a check on catalyst deactivation. Based on these tests, it appears that the catalyst was stable and did not deactivate during the 9 runs.

Based on previous work on a similar type of catalyst that was run under similar conditions on our Berty reactor system, we are confident that the data were free of mass transfer/pore diffusion limitations.

Examination of the parity plot in Figure 4 shows that Equation 1 fits the experimental data well. Nevertheless, the values of the regressed kinetic constants were still changing in Runs 7 and 8 (see Fig. 4), although the values improved as the number of runs increased as indicated by the decrease in the confidence interval with succeeding runs (see Table 3).

Runs 1-9 provide useful kinetic data at one temperature; however, these data are not adequate for establishing a complete set of kinetic parameters or for validating microkinetic models. Similar data sets will need to be obtained at two additional temperatures (at least) for modeling the effects of temperature.

B. CO-TPD study on Unsupported Iron Catalysts

1. CO adsorption/dissociation study on unsupported iron catalysts

CO adsorption and CO-TPD were conducted on samples of an unsupported iron catalyst, 99FeA, prepared by a co-precipitation method reported previously. CO-TPD involved CO adsorption at RT, followed by CO-TPD in pure He gas at 30ºC/min to around 800ºC. CO adsorption was repeated at RT followed by CO-TPD. CO adsorption was subsequently carried out at 100ºC and 150ºC followed by CO-TPD tests. The sample was re-reduced at 600ºC for 12 h between each run. Results are summarized in Table 4 and Figures 6 and 7.

Figure 6 shows CO-TPD profiles on 99FeA samples reduced at 450ºC and 600ºC. The peaks at lower temperature around 117ºC and 199ºC are assigned to desorption of molecular CO, while the peaks at higher temperatures are attributed to recombination of dissociated CO on the iron surface. It is apparent that following reduction at the higher temperature (600ºC) the fraction of molecularly adsorbed CO decreases; the fraction of dissociated CO increases; and the peak for dissociated CO is shifted to lower temperatures, suggesting that recombination of dissociated CO is facilitated relative to the sample reduced at lower temperature. In the first TPD after reduction at 450ºC and adsorption at RT (Figure 6), four peaks are observed; however, after the second

adsorption at RT only two TPD peaks (117ºC and 479ºC) and a small shoulder (579 ºC) are observed. This difference indicates that the TPD to high temperature (~800ºC) and subsequent reduction at higher temeprature eliminates some CO adsorption sites.

The quantities of CO desorbed at 117 and 579ºC from the 99FeA after adsorption at different temperatures are shown in Figure 7 and summarized in Table 4. The area of the peak at 117ºC, assigned to molecularly adsorbed CO, decreases with increasing CO adsorption temperature, while the area of the peak at 579ºC increases with increasing CO adsorption temperature, indicating that CO dissociation is facilitated at higher adsorption temperature and is complete above about 150ºC.

Table 4. Amount of CO adsorbed on 99FeA sample at different adsorption temperatures

Run	Adsorption Temperature	Amount of CO desorbed at various TPD stages (μmol/g cat)			
		117ºC	199ºC	579ºC	752ºC
1	25ºC	4.49	0.73	5.31	3.27
2	25ºC	0.87		0.75	
3	100ºC	0.26		1.20	
4	150ºC	0.09		4.46	

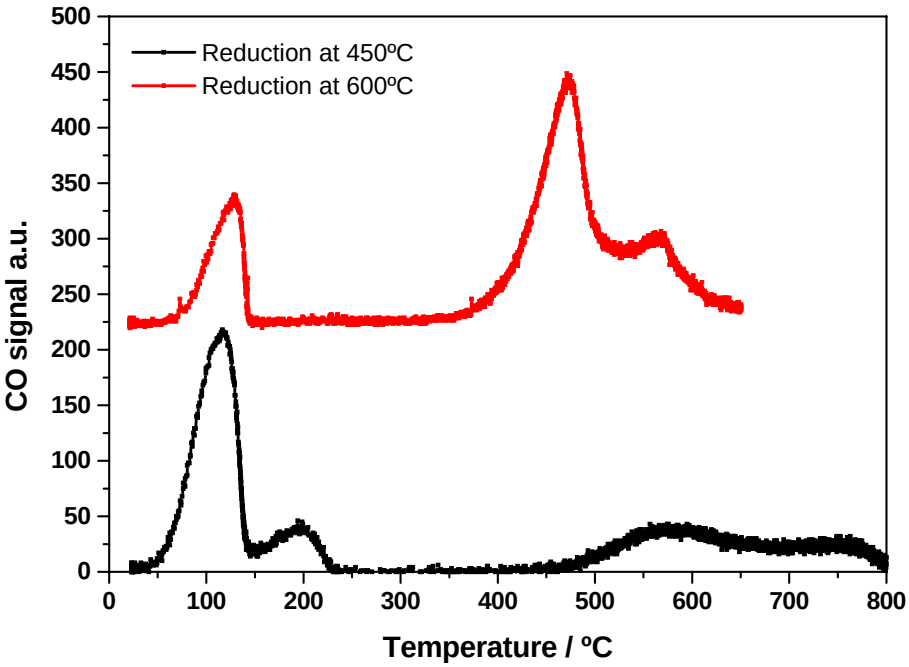

Figure 6. CO-TPD profiles for 99FeA samples reduced at 450 and 600ºC respectively.

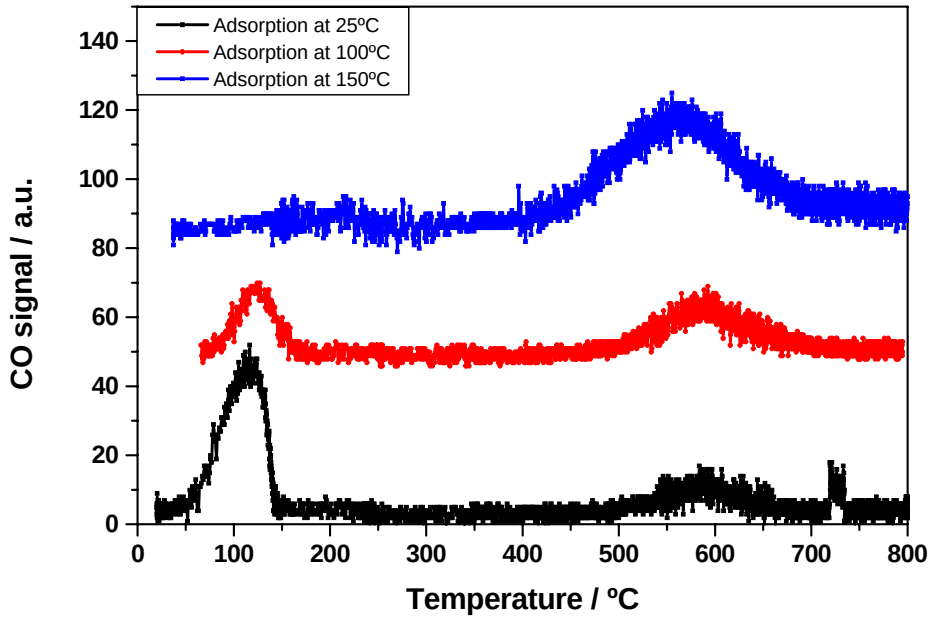

Figure 7. CO-TPD profiles on 99FeA sample after CO adsorption at different temperatures.

2. CO heat of adsorption

Determination of the heat of adsorption for CO on the unsupported iron catalysts involved using the CO-TPD spectra as a function of varying initial coverage. Data analysis is based on an Arrhenius form of the rate constant for adsorption. A linear form involves plotting $\ln(\theta_n/(1-\theta_n))$ versus $1/T_a$. Figure 8 shows the plot of heat of adsorption of CO versus coverage.

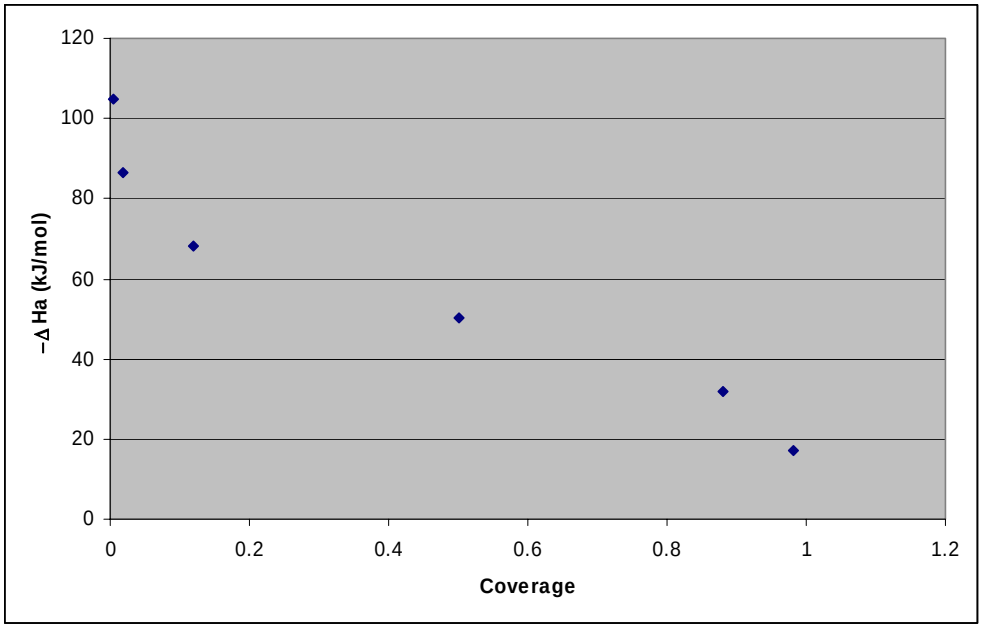

Figure 8. Enthalpy of adsorption of CO on unsupported iron catalysts as a function of coverage.

Table 5 compares the CO heat of adsorption on iron in this work with other studies.

Table 5. CO Heat of Adsorption on SC and PC Fe

	Heat of Adsorption (kJ/mol)	Reference
SC Fe, Calculated	140~200	3
Fe(100), Experimental	100 ± 5	4
PC Fe, Experimental	100	This work

C. Isothermal Hydrogenation on Unsupported Iron Catalysts and Simulation Model Build

1. Isothermal hydrogenation study on unsupported iron catalysts at different temperatures

Isothermal hydrogenation was conducted on unsupported iron catalyst, 99FeA. The sample was pre-reduced at 500ºC for 12 h, and subjected to hydrogenation at different temperatures. The procedure in each run involved the following steps: 25% CO/H_2, 5~10 min (10 min for 200ºC) ⟶ He, 10 min ⟶ 25% H_2/He. The entire experiment was conducted at 1 atm.

Figure 9 shows the results of the isothermal hydrogenation experiments over 99FeA sample at different temperatures. As the syngas treatment and isothermal hydrogenation were carried out at 285ºC, three obvious peaks can be seen on the spectrum. Thus, the carbonaceous species may include include several carbonaceous species including two kind active surface carbon α and β, and at least one bulk carbide. At 200ºC, the intensity of isothermal hydrogenation peaks significantly decrease, while carbonaceous species are similar with the sample treated at 285ºC. However, at the two lowest temperatures, 150ºC and 175ºC, only active surface carbons were formed on surface after syngas treatment. The carbon coverage is less than 1 ML based on the hydrogen chemisorption uptake. Further hydrogenation studies will be conducted at 150ºC.

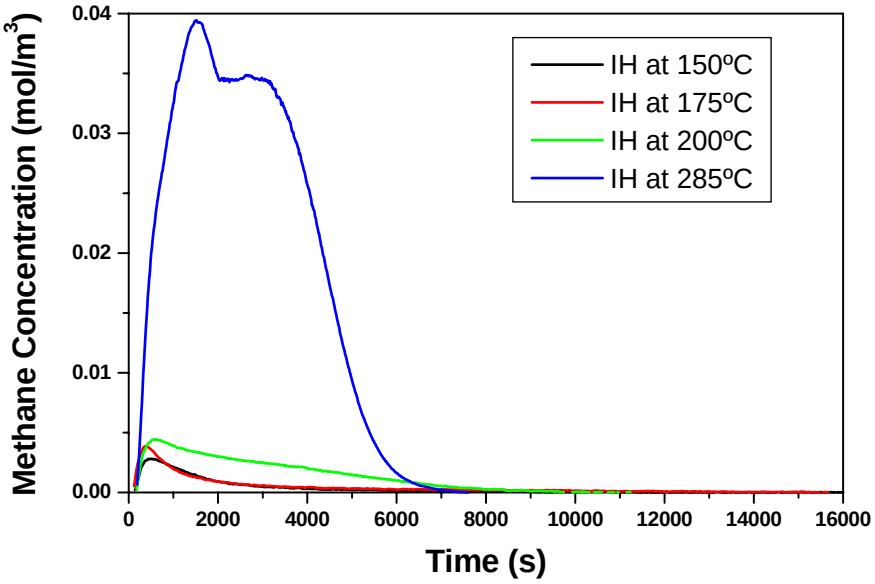

Figure 9. Isothermal hydrogenation spectra of 99FeA samples after pretreatment in syngas.

2. The quantities of surface carbonaceous species after FTS on 99FeAl

The mechanism of methanation of carbonaceous adsorbed species in Fischer Tropsch reaction was hypothesized. Three models based on the types of carbonaceous species involved were proposed: (1) a single site carbon species model (Model 1), a two-site carbon species model (Model 2), and carbene blended with CO insertion model (Model 3). The related elementary steps for each model are listed below in the discussion which follows. A single elementary step is modeled with 2 rate parameters, a frequency factor and an activation energy. The reactor model is represented by partial differential equations in time and space for the components. The equation for each gaseous component i is:

$$\frac{\partial C_i}{\partial t} + \frac{1}{\tau}\frac{\partial C_i}{\partial x} = \frac{\rho_b}{\varepsilon_b} R_{w,i}$$

and the equation for surface component j is represented by:

$$\frac{dL_j}{dt} = R_{w,j}$$

where ρ_b is the bed density in $kg_{cat} \cdot m_{bed}^{-3}$; and τ is the residence time in s, i.e. $\tau = \varepsilon_b V_R / F_v$; ε_b is the bed void fraction.

The above partial differential equation was discretized in space into a uniform grid while an ordinary differential equation solver routine DVODE developed by Livermore National Labs was used to integrate the resulting system of ODE's. Rate constants for each elementary step were estimated using an orthogonal distance regression package ODRPACK. Both DVODE and ODRPACK were integrated into a local Fortran routine that was used to regressed the rate constants from experimental data.

The following sets of elementary steps were used to model isothermal hydrogenation at 175ºC. The equations and parameters for fitting Model 2 are attached by way of example in Appendix 1.

i. Single site carbon species model (Model 1)

The elementary steps of hydrogenation of carbonaceous adsorbed species in Fischer Tropsch reaction to methane in this model are:

$$H_2 + 2s \leftrightarrow 2H - s \quad (1)$$

$$H - s + C - s \leftrightarrow CH - s + s \quad (2)$$

$$H - s + CH - s \leftrightarrow CH_2 - s + s \quad (3)$$

$$H - s + CH_2 - s \leftrightarrow CH_3 - s + s \quad (4)$$

$$H - s + CH_3 - s \leftrightarrow CH_4 + 2s \quad (5)$$

Figure 10 shows the plot of simulated and experimental methane concentration versus reaction time. The agreement between experiment and prediction is poor.

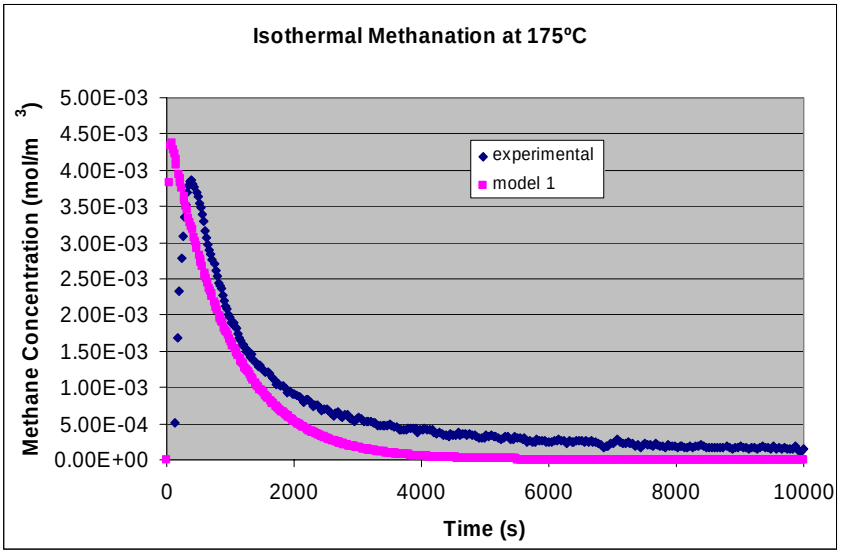

Figure 10. Simulated (model 1) and experimental methane concentration vs. reaction time for the isothermal hydrogenation of carbonaceous species on 99FeA samples after pretreatment in syngas at 175ºC.

ii. Two site carbon species model (Model 2)

Given the broad peak for the experimental data in Figure 10, it is likely that adsorbed carbon atoms are bound to sites of differing coordination (hence surface energy) on the irregular surfaces of small iron crystallites. We have chosen to approximately model this phenomenon by postulating that two different carbon species, α_1 and α_2, having different binding energies, are formed on the surface during FT reaction; it is expected that both undergo reaction to methane in the hydrogenation process. The simple kinetic model based on these two carbon species can be written as:

$$H_2 + 2s \leftrightarrow 2H - s \qquad (6)$$

$$H - s + C_{\alpha 1} - s \leftrightarrow CH - s + s \qquad (7\text{-}1)$$

$$H - s + C_{\alpha 2} - s \leftrightarrow CH - s + s \qquad (7\text{-}2)$$

$$H - s + CH - s \leftrightarrow CH_2 - s + s \qquad (8)$$

$$H - s + CH_2 - s \leftrightarrow CH_3 - s + s \qquad (9)$$

$$H - s + CH_3 - s \leftrightarrow CH_4 + 2s \qquad (10)$$

While the simulated curve for Model 2 (Fig. 11) fits the experimental data better than for Model 1 (Fig. 10) it is still not adequate; this result suggests that in addition to surface carbonaceous species other species such as CH, CHO, etc, also coexist on the surface.

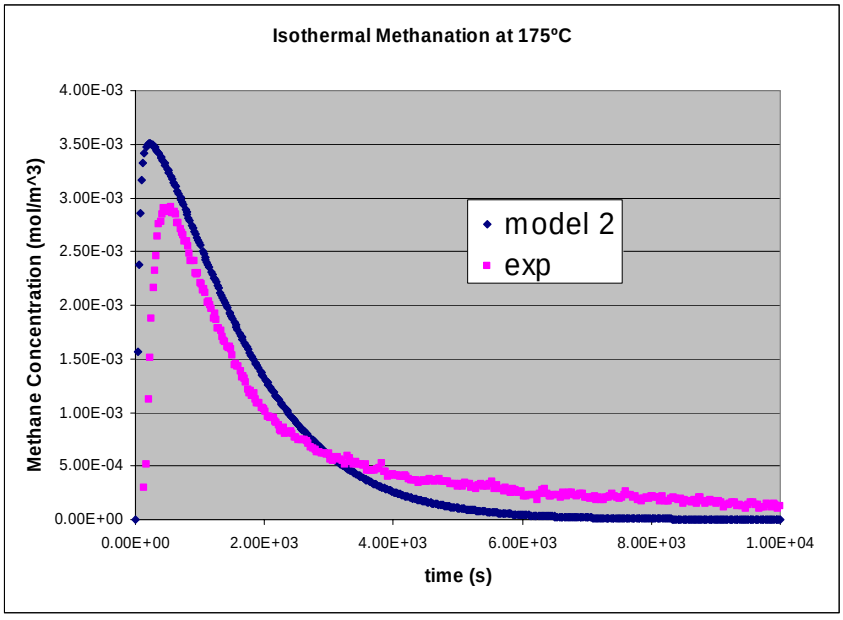

Figure 11. Simulated (model 2) and experimental methane concentration vs. reaction time for the isothermal hydrogenation of carbonaceous species on 99FeA samples after pretreatment in syngas at 175ºC.

iii. Carbene blended with CO insertion model (model 3)

Considering the complexity of the surface species after pretreatment in syngas, we proposed Model 3 involving 13 elementary steps and 10 surface species, i.e., H, CH, CH_2, CH_3, CHO, CH_2O, CH_3O, OH, O, CO. It involves hydrogenation via both CH_x and CHO species. Figure 12 shows the plot of simulated (Model 3) and experimental methane concentration versus reaction time. While Model 3 fits the experimental data better than Models 1 and 2, there is still room for improvement. We have recently found that broadening of the experimental curve occurs as a result of axial and radial dispersion. We are expecting to minimize this problem through redesign of the TPD reactor.

$$H_2 + 2s \leftrightarrow 2H - s \quad (11)$$
$$CHO - s + H - s \leftrightarrow CH_2O - s + s \quad (12)$$
$$H - s + C - s \leftrightarrow CH - s + s \quad (13)$$
$$H - s + CH - s \leftrightarrow CH_2 - s + s \quad (14)$$
$$H - s + CH_2 - s \leftrightarrow CH_3 - s + s \quad (15)$$
$$H - s + CH_3 - s \leftrightarrow CH_4(g) + 2s \quad (16)$$
$$CHO - s + CH_3 - s \leftrightarrow CH_3CHO(g) + 2s \quad (17)$$
$$HO - s + H - s \leftrightarrow H_2O(g) + 2s \quad (18)$$
$$O - s + H - s \leftrightarrow OH - s + s \quad (19)$$
$$CH_2O - s + H - s \leftrightarrow CH_3O - s + s \quad (20)$$
$$CH_3O - s + H - s \leftrightarrow CH_3O - s + OH - s \quad (21)$$
$$CO - s + s \leftrightarrow C - s + O - s \quad (22)$$
$$CO - s + OH - s \leftrightarrow CO_2(g) - s + H - s + s \quad (23)$$

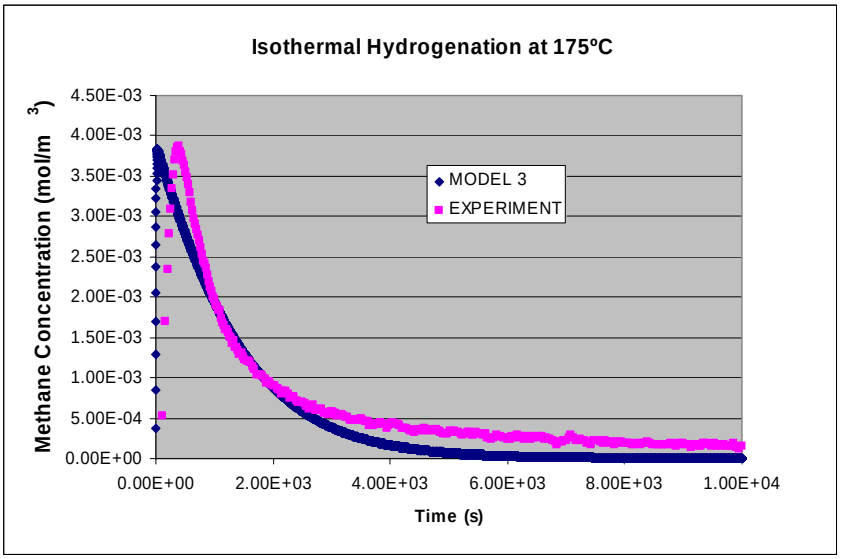

Figure 12. Simulated (Model 3) and experimental methane concentration vs. reaction time for isothermal hydrogenation of carbonaceous species on 99FeA samples after pretreatment in syngas at 175ºC.

Results and Discussion based on First Principles Calculations

In the initial stages of this project we focused our efforts on completing a comprehensive study on the thermochemistry and kinetics of the elementary steps for the Fischer Tropsch Synthesis (FTS) on a variety of model systems. The very first system we studied was a model of an unpromoted Fe catalyst, namely the Fe(110) facet, simply because for a Fe catalyst particle, the (110) would be the thermodynamically most stable, and therefore, dominant facet. FTS catalysts frequently employ Pt promoters and hence our next investigation focused on an Fe(110) facet with a Pt adatom adsorbed on them [represented henceforth as the Fe^{Pt} system which corresponds to a ¼ ML of Pt on the Fe(110) surface]. Furthermore, catalytic activity of FTS Fe catalysts has frequently been correlated with the formation of a Carbide phase and an Fe(110) facet with sub-surface Carbon [denoted as Fe_C] allowed us to probe the effects of Carbon on the thermochemistry and kinetics of FTS elementary steps. For reference, Figure 13 shows schematics of all the three systems studied so far (Fe(110), Fe^{Pt}, and Fe_C). These studies provided a variety of important insights into the behavior of Fe based FTS catalysis, details of which have been documented in our previous annual reports. In the interest of brevity, this section of our current report concentrates on our findings in the third year of the project spending only a limited time in summarizing and contrasting the current results with our previous findings where warranted.

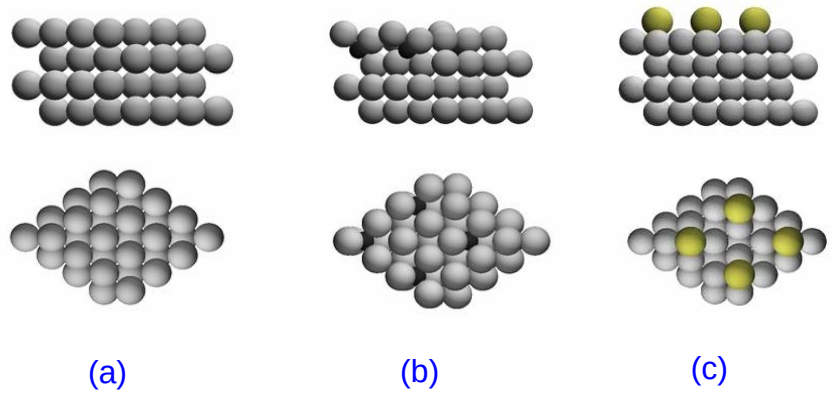

Figure 13 Some model systems considered for first-principles studies of FTS on Fe catalysts. (a) Fe(110), (b) Fe_C(110) which is a Fe(110) slab with an additional ¼ ML of C in the first sub-surface layer, (c) Fe^{Pt}(110) which is a Fe(110) slab with a ¼ ML of Pt adatoms on the surface. Top panel gives the cross-section view; bottom panel gives top-views of corresponding slabs.

As we embarked into our studies in the third year of the project a key goal before us was to analyze the FTS elementary steps on a defected Fe surface. A number of possibilities existed for candidate systems but before we made a decision we had to critically evaluate the candidates in order to select viable options that met some key requirements: We needed a system that would closely represent the experimental situation but at the same time be amenable to modeling with a reasonable unit cell size. The first system we investigated was a **"stepped Fe(110)"** surface generated by removing a row of Fe surface atoms which then has a pronounced step on the surface. Figure 14 shows a schematic of this **"stepped Fe(110)"** surface which we then employed to obtain the Binding Energies(BE's) of the various intermediates and stable species that are involved in our scheme of elementary steps to model FTS. Our calculations showed that in most cases the species bind with a strength that is comparable to the original Fe(110) facet. This is not surprising noting the very similar surface structure of Fe(110) and the **"stepped Fe(110)"** as is evident from the panels of Figures 13 and 14.

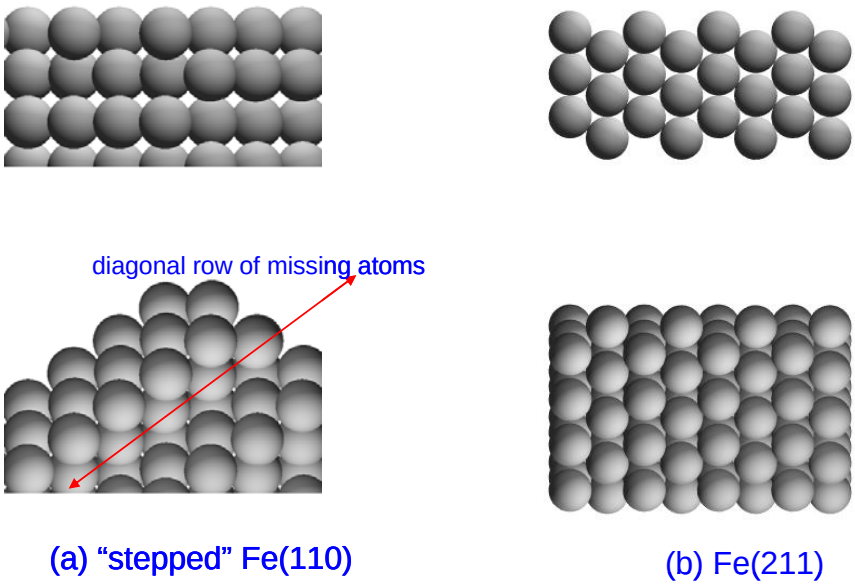

Figure 14 Two models for a defected Fe surface. (a) "stepped" Fe(110) which has a missing row of atoms from a native Fe(110) facet; (b) Fe(211) Top panel gives the cross-section view; bottom panel gives top-views of corresponding slabs.

We then expanded our search for a "defected Fe surface" to include other candidates that are specific facets of the Fe bulk lattice that exhibit pronounced steps and terraces. Based on existing literature we identified Fe(321) and Fe(211) as potential candidates and finally decided to select Fe(211) as our model system for further studies [Refer to Figure 14 for a schematic view of this facet]. Surprisingly, there exists very little work in literature on this facet, but since

it has a surface energy only slightly higher than the Fe(110) facet, it would be very stable and hence we thought as deserving of a more detailed analysis. Using state-of-the-art First-Principles DFT planewaves-based methods we proceeded to calculate the Binding Energies (BE's) and site preferences of the 19 major surface intermediates that are involved in our FTS model. These include several classes of species:

- The single carbon species: C, CH, CH_2 , CH_3 and CH_4
- Larger C_2 intermediates including: C-CH_3, CH_3-CH, CH_2-CH, CH_3-CH_2, C_2H_2, C_2H_4 and C_2H_6
- Other associated species and intermediates including: CO, CO_2, O, H, OH, H_2O,

Table 6 summarizes the BE's of species on the Fe(211) surface which are also represented in Figure 15 in a graphical format (arranged in descending order of the magnitude of their BE's). Our first-principles studies also yield other fundamental information regarding the binding of these varied species on Fe; one of the more interesting aspects that can be probed on a molecular level is concerned with the site-preferences of the species on this surface. We determined the preferred binding sites of all the species considered on the Fe(211) surface. Taking into account the relative low-symmetry of the stepped (211) facet a larger variety of sites must be tested when compared to the earlier Fe(110) facet. In many cases the preferred adsorption geometry is similar to that obtained on Fe(110), but in a significant number of cases interesting differences are observed. Figure 16 allows us to observe several such configurations in greater detail. Species like H, O and CO bind in similar configurations on Fe(110) and on Fe(211); others including CO, OH and CO_2 exhibit substantially different configurations (including tilted configuration in some cases).

A comparison with the corresponding Binding Energies (BE) on the Fe(110) facet might be useful and Figure 17 provides a graphical representation of this information. For a large part, these binding energies on Fe(211) follow the same trend established on Fe(110), yet there are significant deviations superimposed on the underlying trend. The magnitude of these deviations (between BE of a species on the (110) and (211) facets) spans a fairly wide range, reaching a maximum of about 1 eV for CO_2. These variations cannot be discounted and might, in fact, play a role in modifying the reactivity of Fe catalyst nanoparticles.

Species	BE (eV)
C	-7.34
CH	-6.66
C-CH	-6.17
O	-5.80
CCH_3	-5.63
$C\text{-}CH_2$	-4.81
OH	-4.02
CH_2	-3.99
CH_3CH	-3.70
CH_2CH	-3.67
H	-2.85
C_2H_2	-2.83
CH_3	-2.20
CO	-2.05
C_2H_5	-1.92
CO_2	-1.48
C_2H_4	-1.31
H_2O	-0.58
C_2H_6	-0.06
CH_4	-0.05

Table 6 Summary of Binding Energies (BE) of various species on Fe(211).

The next stage in our calculations was the calculation of the vibrational frequencies of the preferred adsorption configurations of all species studied on Fe(211). These results are useful because the vibrational frequencies can then be used for determining the pre-exponential factors, and entropy changes for the various surface elementary reaction steps. Furthermore, knowledge of the vibrational frequencies also allows us to apply Zero Point Energy (ZPE) corrections to the BEs (Binding Energies) predicted by our models. Note that we have in the past established a database of vibrational frequencies of species adsorbed on Fe(110), Fe_C(110) and Fe^{Pt}(110); the addition of the Fe(211) frequencies extends this data and provides a useful connection with experimental vibrational frequency work (e.g.: IRAS, HREELS, etc).

Having completed a comprehensive study of the thermodynamics of FTS on Fe(211) our next goal was to analyze Minimum Energy Paths (MEP) and to determine the activation energy barriers for the various elementary steps on Fe(211). In all the systems we had studied so far, our calculations indicated that CO dissociation is a rather difficult step (relative to other steps, it has high activation energy barrier). It was therefore an ideal candidate step to start our kinetic calculations on, and further could provide important information whether the current stepped model surface viz. Fe(211) could do any better. Indeed, we did find that CO dissociation is more

facile on the stepped Fe(211) surface when compared to Fe(110) [a barrier of 1.16 eV on Fe(211) vs. 1.52 eV on Fe(110)]. This is an important finding as it might allow us to reconcile our models to the high FTS Turnover frequencies (TOFs) measured in experiments. Other options for facile CO dissociation do exist, including the Boudard reaction [CO + CO → CO_2 + C] which makes for a promising alternative to direct CO dissociation. Unfortunately, because of limitations with CPU time we were not able to make a detailed analysis of these alternative CO-dissociation routes.

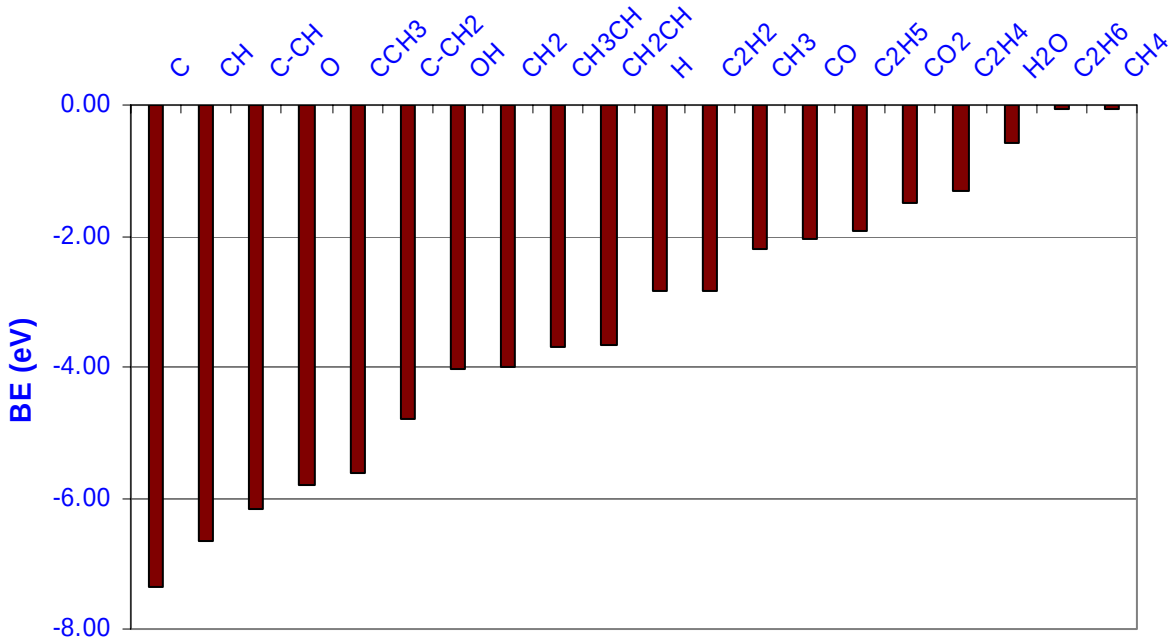

Figure 15 Trends in Binding Energy (BE) of species on Fe(211). Species to the left of the chart are the strongest binding (eg. C), while those to the right bind the weakest (eg. CH_4). All energies are referred to gas phase species at infinite separation from the Fe(211) slab.

We then proceeded with calculations to evaluate the PES (Potential Energy Surface) for the early FTS steps (up o CH_4 formation) on Fe(211). The steps involved are:

- $C_{(a)} + H_{(a)} \rightarrow CH_{(a)}$
- $CH_{(a)} + H_{(a)} \rightarrow CH_{2(a)}$
- $CH_{2(a)} + H_{(a)} \rightarrow CH_{3(a)}$
- $CH_{3(a)} + H_{(a)} \rightarrow CH_{4(a)}$

In accordance with the protocol adopted throughout the course of this project we do include the effects of surface relaxation in our calculations, which makes the calculations expensive [especially on a high index surface like the (211)], but more realistic. Our calculations indicated that for the most part, the barrier remained substantially unchanged irrespective of the facet

under consideration [Fe(110) vs Fe(211)] for all the steps in this series. Thus, Fe(211) allowed for facile CO dissociation while most of the other steps remained unaffected in terms of their activation energy barrier. This is an important finding, and the respective comparison is highlighted in Figure 18.

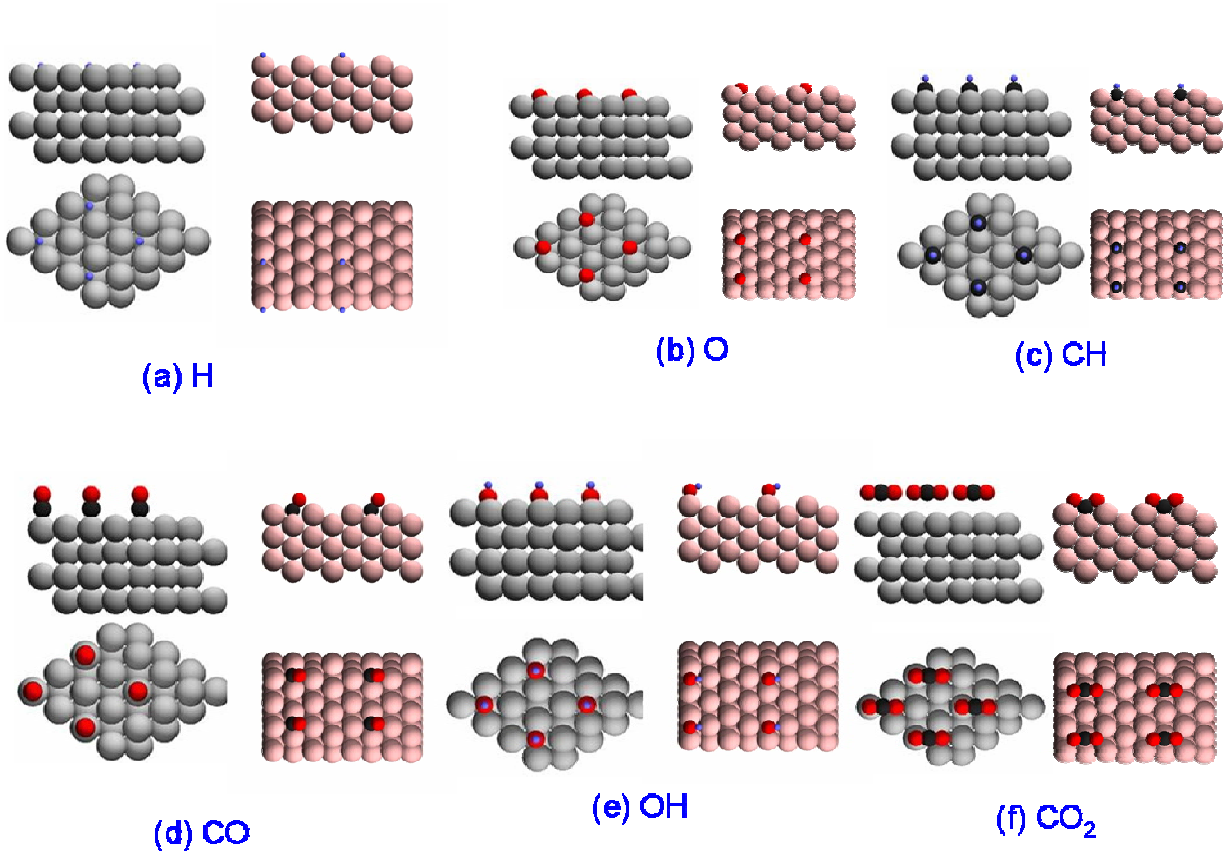

Figure 16 Comparison of site-preferences of species adsorbed on Fe(110) and Fe(211). In each panel, right image corresponds to Fe(211) (also color coded red for clarity), left image to Fe(110). Atoms are colored as follows: Oxygen-red, Hydrogen-blue, Carbon-black.

Our model of FTS is comprised of a fairly complex network of steps as shown in Figure 19. Unfortunately, we did not have the time to conduct a detailed kinetic analysis of all the remaining elementary steps on Fe(211) (except for: CO dissociation and the early steps up to CH_4 formation, which are highlighted in Figure 19). An alternative way of looking at the problem is to classify the steps into broad classes based on the type of bond-formation / bond-breaking involved in the particular step (see Figure 20). It is obvious that, in general, there are multiple competing pathways for production of most of the C_2 and higher intermediates. Only on completion of a kinetic analysis of all the steps involved, and possibly on construction of an appropriate microkinetic model can a final judgment as to the relative importance of the various steps be made. Nevertheless, our studies in the last year of the project were very fruitful in elucidating the behavior (both thermodynamic and kinetic) of FTS elementary steps on stepped

Fe surfaces. We contrasted these properties with the Fe(110) surface and reached the conclusion that CO dissociation in particular would be favored on the stepped surface whereas the other early FTS steps would occur at least as easily on Fe(211) as on Fe(110).

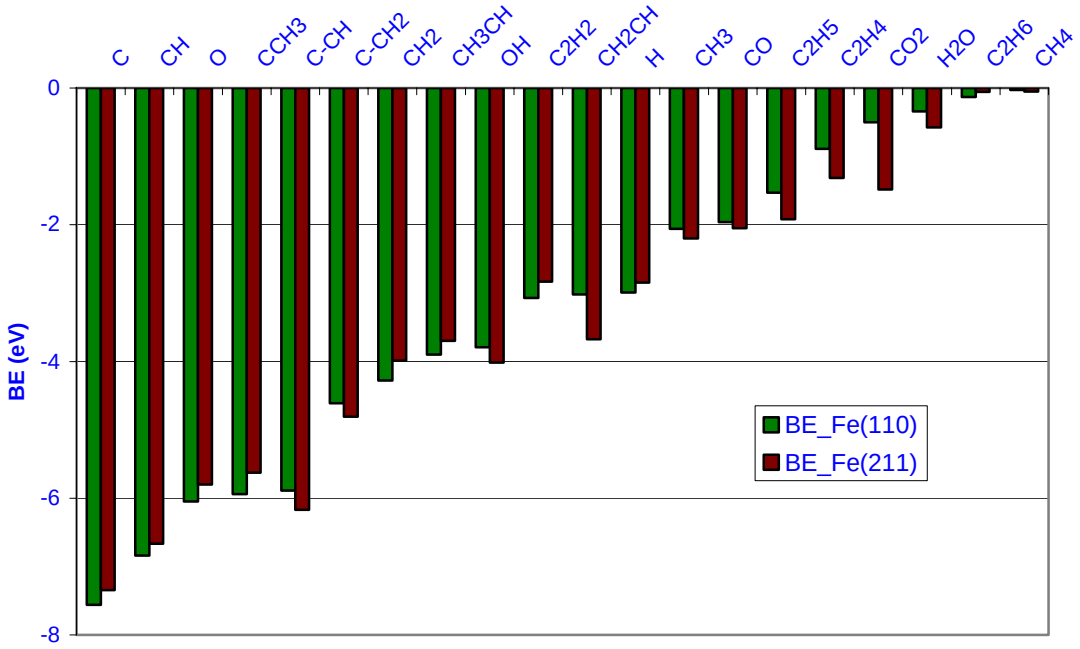

Figure 17 Comparative Trends in Binding Energy (BE) on Fe(110) vs Fe(211)

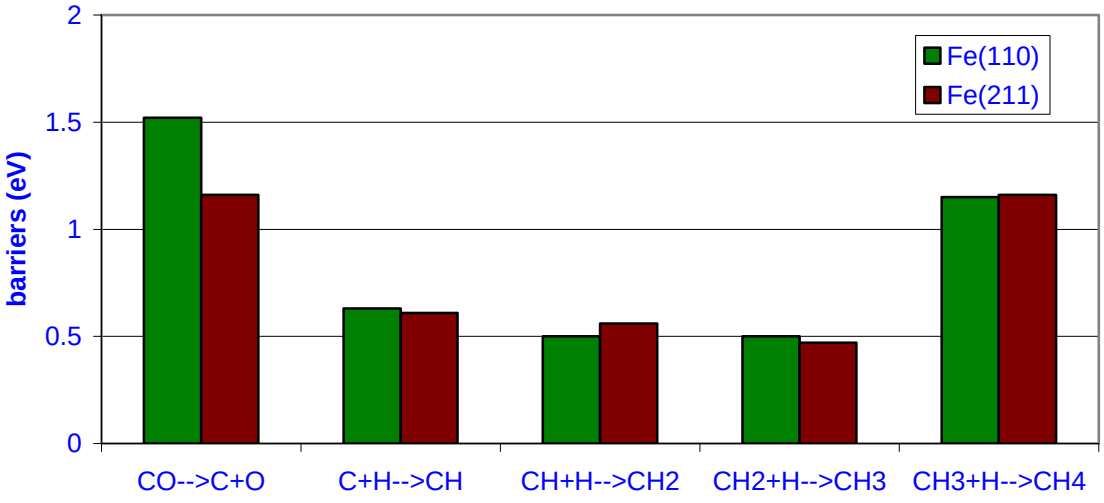

Figure 18 Comparison of the activation energy barriers for the early steps of FTS on Fe(110) and Fe(211).

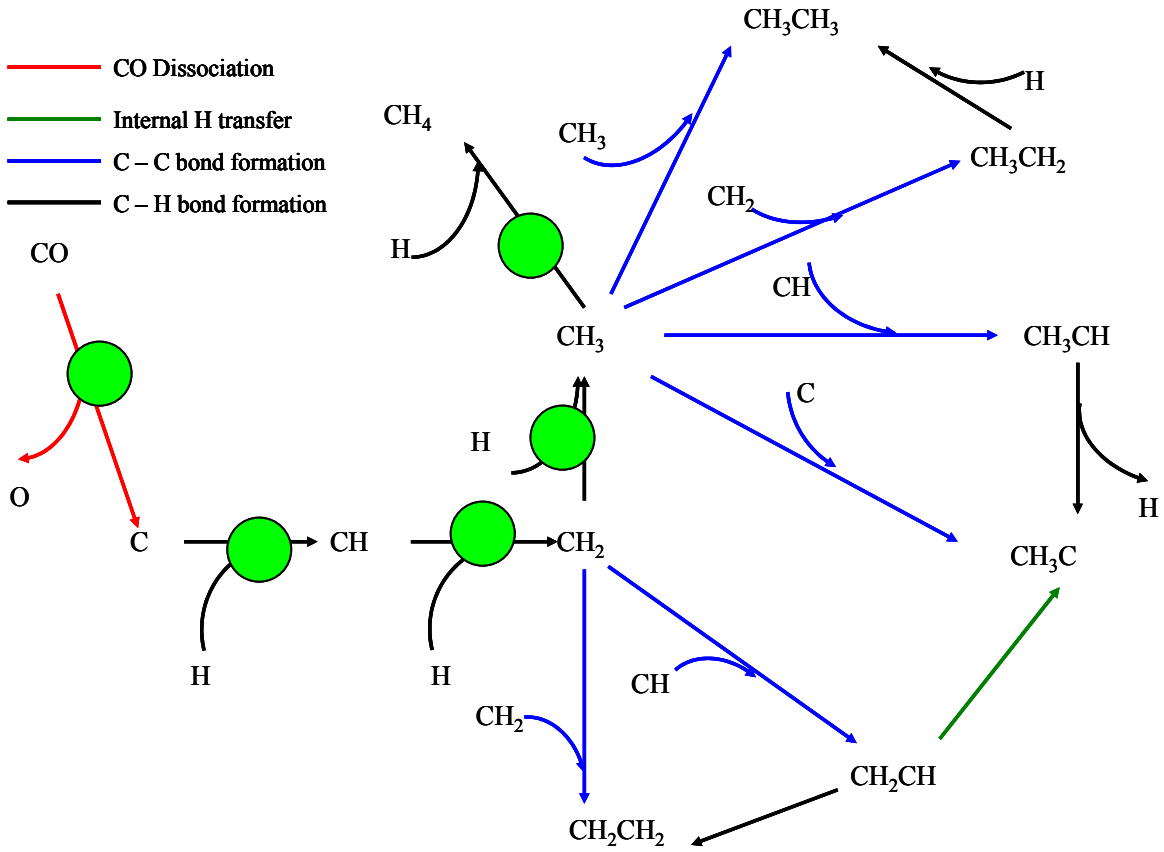

Figure 19 Reaction Network for FTS on Fe(110) and Fe(211) surfaces. Steps highlighted by green circles denote the elementary steps whose barrier has already been evaluated using first-principles methods on Fe(211). For the remaining steps thermochemistry has been calculated but minimum energy path calculations have not been completed yet. For Fe(110) the entire network of steps has been studied, both for thermochemistry and kinetics.

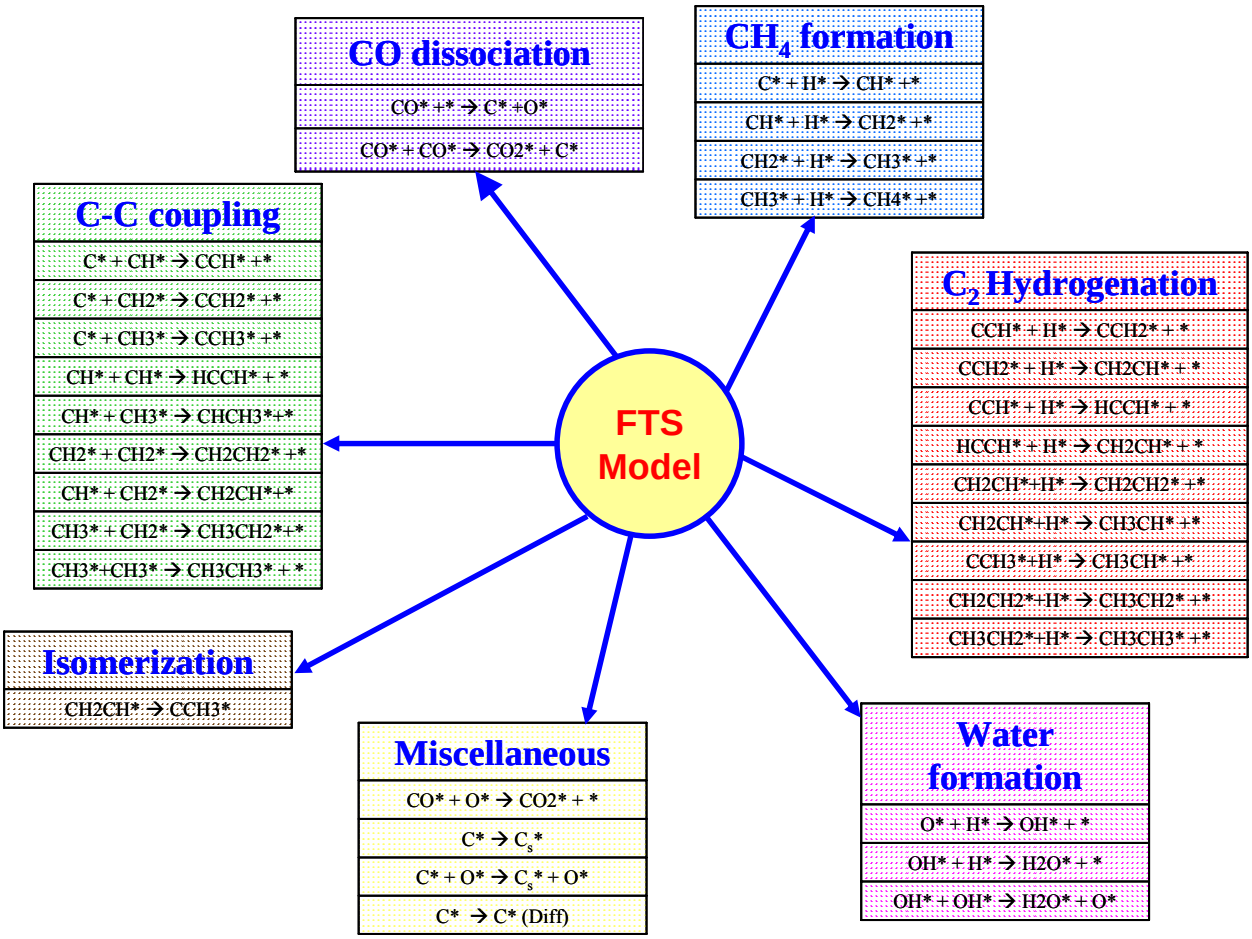

Figure 20 Functional classification of steps involved in our FTS model on Fe(110) and Fe(211)

Methods

All calculations were performed using the first-principles total energy calculation code DACAPO. Adsorption is allowed on only one of the two surfaces of the slab and the electrostatic potential is adjusted accordingly. Calculations are all spin-polarized. The Fe(110) surface is modeled by a (2x2) unit cell, corresponding to a ¼ ML coverage for all individual adsorbates. Fe(211), on the other hand, is a more open stepped surface and requires a larger (2x4) unit cell with a total of 3 equivalent layers(24 atoms). Since the Fe(110) and Fe(211) surfaces considered are rather open, surface-perturbation could have a significant effect on the adsorption properties of the various species; hence Fe(110) is modeled using a four layer slab with the top two layers fully relaxed [details differ slightly for Fe(211)]. Kohn-Sham one-electron valence states are expanded in a basis of plane waves with kinetic energy below 25 Ry. The exchange-correlation energy and potential are described by the generalized gradient approximation (GGA-PW91); the ionic cores are described by ultrasoft pseudopotentials. The surface Brillouin zone is sampled with a 4x4x1 *k* point set. The calculated equilibrium PW91 lattice constant for bulk Fe is: a = 2.85 Å, in good agreement with the experimental value of 2.87 Å. The minimum energy reaction paths of various elementary steps are studied using the Climbing-Image Nudged Elastic Band (CI-NEB) method, a state-of-the-art iterative method. The existence of saddle points is further

verified by the existence of a single imaginary vibrational frequency for the optimized transition state.

Future work based on First Principles Calculations

1. Completion of kinetic analysis and evaluation of the MEP and barriers for all the elementary FTS steps on Fe(211). That would allow for a more detailed comparison with Fe(110) especially with respect to product yields and distributions of C_2 and higher species.
2. Construction of a comprehensive microkinetic model for FTS on Fe(211) and Fe(110) that allows us to put the relative contribution of various competing pathways and turnover-frequencies (TOF's) on a quantitative basis.
3. Study of K-promotion of Fe-catalyzed FTS.

Conclusions

1. CO dissociation occurs readily on polycrystalline Fe at 25-100°C and is completely dissociated above about 150°C. Accordingly CO dissociation is probably not the rate determining step in FT reaction.
2. The heat of CO adsorption on polycrystalline Fe is around 100 kJ/mol.
3. After FT reaction at temperatures above about 200°C, the Fe surface of 99% Fe contains a complex distribution of carbonaceous species. After reaction at 150-175°C the predominant surface species are active carbons, CH_x, and CHO_x species.
4. Hydrogenation of the surface species following reaction is modeled by as many as a dozen (or more) elementary steps and 10 different surface species.
5. A sequential design procedure using a D-optimal method resulted in precise kinetic parameter estimates at one temperature after only 9 runs.
6. Density Functional Theory (DFT) calculations revealed that the Binding Energies (BE's) of most species on the stepped Fe(211) surface parallel the trends observed on the Fe(110) surface but there are significant variations imposed on the underlying trends. The reaction network we established for FTS is relatively complex with 32 elementary steps involving 19 species and we made significant progress in characterizing the network with respect to its thermochemistry and kinetics. CO dissociation was observed to be a particularly facile reaction on Fe(211) in comparison to all the previously studied Fe systems.

References

1. G. P. Van der Laan, A. A. C. M. Beenackers "Kinetics and selectivity of the Fischer-Tropsch synthesis: A literature review" Catal. Rev. –Sci. Eng. 41 (1999) 255-318.
2. C.H. Bartholomew and R. J. Farrauto, "Fundamental of Industrial Catalytic Processes".
3. T.C. Bromfield, D. C. Ferre, and J.W. Niemantsverdriet, ChemPhysChem, 6, 254 (2005).
4. T.J. Vink, O.L. Gijzeman, J.W. Geus, Surf.Sci.,150,14 (1985).

List of Presentations

1. Brian L. Critchfield, Uchenna Paul, Calvin H. Bartholomew, and H. Dennis Tolley, "Statistically-designed study of the reaction kinetics of Fischer-Tropsch synthesis on a $FePt/La_2O_3/Al_2O_3$/monolith catalyst," presented at the Annual Meeting of the Western States Catalysis Club, Boulder, Colorado, February 24, 2006.

2. Hu Zou and Calvin H. Bartholomew, "CO Adsorption/Dissociation and Carbon Hydrogenation on Unsupported Iron Fischer-Tropsch catalysts," presented at the Annual Meeting of the Western States Catalysis Club, Boulder, Colorado, February 24, 2006.

3. Hu Zou, Uchenna Paul, and Calvin H. Bartholomew "CO Adsorption/Dissociation and Carbon Hydrogenation on Iron Fischer-Tropsch Catalysts" presented at the Annual Meeting of the AIChE, San Francisco, November 12-17, 2006.

4. Rahul P. Nabar, Amit A. Gokhale, and Manos Mavrikakis, "A Theoretical Comparative Study of Fischer-Tropsch Synthesis on Fe and Co Surfaces", presented at the Annual Meeting of the AIChE, San Francisco, November 12-17, 2006.

Appendix 1

[1] d(Y1)/d(t) = -(Y1-YH2_0)/(TAU*DELTA)+ROH_BED*(-K1*Y1*Y5^2+K_1*Y4^2)/EB
H2 CONCENTRATION AT REACTOR EXIT
[2] d(Y2)/d(t) = -(Y2-YCH4_0)/(TAU*DELTA)+ROH_BED*(CH4RATE_ALPHA1+CH4RATE_ALPHA2)/EB
METHANE CONCENTRATION AT SECOND NODE
[3] d(Y3)/d(t) = -K2*Y3*Y4+K_2*Y6
Alpha 1 CARBON CONCENTRATION AT SECOND NODE
[4] d(Y4)/d(t) = HRate_1+HRate_2_ALPHA1+HRate_2_ALPHA2
SURFACE H CONCENTRATION AT SECOND NODE
[5] d(Y5)/d(t) = VRate_1+VRate_2_ALPHA1+VRate_2_ALPHA2
VACANT SITE CONCENTRATION AT SECOND NODE
[6] d(Y6)/d(t) = K2*Y3*Y4-K_2*Y6-K3*Y6*Y4+K_3*Y7*Y5
Alpha 1 SURFACE CH CONCENTRATION AT SECOND NODE
[7] d(Y7)/d(t) = K3*Y6*Y4-K_3*Y7*Y5-K4*Y7*Y4+K_4*Y8*Y5
Alpha 1 SURFACE CH2 CONCNETRATION AT SECOND NODE
[8] d(Y8)/d(t) = K4*Y7*Y4-K_4*Y8*Y5-K5*Y8*Y4+K_5*Y2*Y5^2
Alpha 1 SURFACE CH3 CONCENTRATION AT SECOND NODE
[9] d(Y9)/d(t) = -K7*Y9*Y4+K_7*Y10
ALPHA 2 CARBON CONCENTRATION
[10] d(Y10)/d(t) = K8*Y9*Y4-K_8*Y10-K9*Y10*Y4+K_9*Y11*Y5
ALPHA 2 SURFACE CH CONCENTRATION
[11] d(Y11)/d(t) = K8*Y10*Y4-K_8*Y10*Y5-K9*Y11*Y4+K_9*Y12*Y5
ALPHA 2 CH2 SURFACE CONCENTRATION
[12] d(Y12)/d(t) = K9*Y11*Y4-K_9*Y12*Y5-K10*Y12*Y4+K_10*Y2*Y5^2
ALPHA 2 CH3 CONCENTRATION
[13] HRate_1 = 2*(K1*Y1*Y5^2-K_1*Y4^2)
Surface H formation from rxn 1
[14] HRate_2_ALPHA1 = -K2*Y3*Y4+K_2*Y6-K3*Y6*Y4+K_3*Y7*Y5-K4*Y7*Y4+K_4*Y8*Y5-K5*Y8*Y4+K_5*Y2*Y5^2
Surface H rate for reactions 2 to 5 based on Alpha 1 carbon
[15] HRate_2_ALPHA2 = -K7*Y9*Y4+K_7*Y10-K8*Y10*Y4+K_8*Y11*Y5-K9*Y11*Y4+K_9*Y12*Y5-K10*Y12*Y4+K_10*Y2*Y5^2
H RATE DUE TO ALPHA 2
[16] VRate_1 = 2*(-K1*Y1*Y5^2+K_1*Y4^2)
Vacant site rate from rxn 1
[17] VRate_2_ALPHA1 = K3*Y6*Y4-K_3*Y7*Y5+K4*Y7*Y4-K_4*Y8*Y5+2*(K5*Y8*Y4-K_5*Y2*Y5^2)
Vacant site rate for ratios 2 to 5 based on Alpha 1 carbon
[18] VRate_2_ALPHA2 = K8*Y10*Y4-K_8*Y11*Y5+K9*Y11*Y4-K_9*Y12*Y5+2*(K10*Y12*Y4-K_10*Y2*Y5^2)
VACANT SITE RATE DUE TO ALPHA 2
[19] CH4RATE_ALPHA1 = K5*Y8*Y4-K_5*Y2*Y5^2
METHANE RATE FROM ALPHA1
[20] CH4RATE_ALPHA2 = K10*Y12*Y4-K_10*Y2*Y5^2
CH4 RATE FROM ALPHA 2
[21] EB = 0.45
BED VOID FRACTION
[22] ROH_BED = 500
BED DENSITY (KG/M^3)
[23] DELTA = 1.0
SPACE STEP SIZE
[24] TAU = 0.134
RESISTANCE TIME (sec)
[25] YCH4_0 = 0
INLET CONCENTRATION OF METHANE
[26] YH2_0 = 7.2
INLET H2 CONCNETRATION (MOL/M^3)
[27] K1 = 2.291E-1
FORWARD RATE CONSTANT OF HYDROGEN

[28] K_1 = 11.755E0
BACKWARD RATE CONSTANT OF HYDROGEN
[29] K2 = 1.5652771
FORWARD RATE CONSTANT OF CARBON REACTING WITH HYDROGEN ON THE SURFACE
[30] K_2 = 0.076868
BACKWARD RATE CONSTANT OF CARBON REACTING WITH HYDROGEN ON THE SURFACE
[31] K3 = 1.5724223
FORWARD RATE CONSTANT OF CH REACTING WITH HYDROGEN ON THE SURFACE
[32] K_3 = 0.717395
BACKWARD RATE CONSTANT OF CH REACTING WITH HYDROGEN ON THE SURFACE
[33] K4 = 1.1914877
FORWARD RATE CONSTANT OF CH2 REACTING WITH HYDROGEN ON THE SURFACE
[34] K_4 = 0.8925375
BACKWARD RATE CONSTANT OF CH2 REATING WITH HYDROGEN ON THE SURFACE
[35] K5 = 1.0848145
FORWARD RATE CONSTANT OF CH3 REACTING WITH HYDROGEN ON THE SURFACE
[36] K_5 = 1.01325672
BACKWARD RATE CONSTANT OF CH3 REACTING WITH HYDROGEN ON THE SURFACE

Appendix 2 Abstracts of Presentations

1. Statistically-designed study of the reaction kinetics of Fischer-Tropsch synthesis on a $FePt/La_2O_3/Al_2O_3$/monolith catalyst

Brian L. Critchfield[1], Uchenna Paul[1], Calvin H. Bartholomew[1], and H. Dennis Tolley[2]
1. BYU Catalysis Lab, Department of Chemical Engineering; 2. Department of Statistics
Brigham Young University, 350 CB, Provo, UT 84602, email: bartc@byu.edu

The reaction kinetics of Fischer-Tropsch synthesis [$CO + 2\ H_2 \rightarrow (1/n)\ C_nH_{2n} + H_2O$] on Fe catalysts has been well studied; indeed, more than a dozen papers report reaction rate expressions and kinetic parameters [1]. However, in several of the previous studies, experimental conditions and catalyst properties were chosen without adequate regard to potential effects on reaction rate of heat/mass transport disguises and catalyst deactivation. These problems could have been avoided through adherence to previously published guidelines [1, 2]. Use of a gradientless CSTR reactor instead of a fixed bed would have also avoided some previous experimental problems.

It is most surprising that none of the previous kinetic studies FTS on Fe incorporated a rigorous statistical experimental design while few studies used accepted statistical methods to regress and evaluate the significance of their fitted parameters. Since design of experiment (DOE) methods are readily available in the literature and have been shown to enable (1) reduction of the number of experiments, (2) determination of fitted parameters with much greater accuracy, and (3) evaluation of interactions between variables, it is a wonder they are not being used. The failure to use accepted, widely-accessible methods for regressing and evaluating statistical significance of rate data and rate models is simply unacceptable as a published work.

We will present the results of a statistically-designed set of experiments, involving sequential DOE, to determine reaction kinetics of FTS on a $FePt/La_2O_3$-Al_2O_3 catalyst. This catalyst was coated on a ceramic, cordierite, cellular monolith (Celcor—Corning Inc.) to facilitate collection of rate data in the absence of pore-diffusional restrictions; the catalyst was designed to be and was, in fact, stable over weeks of operation. Data were collected in a gradientless, stirred-gas recycle Berty reactor to minimize effects of heat and mass transport at conditions representative of commercial operation. Rates of hydrocarbon production were fitted by nonlinear regression to various shifting-order rate expressions (e.g. Langmuir-Hinshelwood) derived from a widely accepted sequence of elementary steps. While several expressions were found to fit the data well, an expression of the form

$$r_{C_{2+}} = \frac{\mathrm{A}\, P_{CO}^{0.67}\, P_{H_2}^{0.83}}{\left(1 + \mathrm{D}\, P_{CO}^{0.67} P_{H_2}^{0.33}\right)^2}$$

provided the best fit to the data. The results of the nonlinear regression of the data and the statistical evaluation of the data and fitted parameters will be presented in some detail.

References

1. C.H. Bartholomew and R.J. Farrauto, *Fundamentals of Industrial Catalytic Processes,* Wiley 2006.
2. F. H. Ribeiro, A. E. Schach von Wittenau, C. H. Bartholomew, and G. A. Somorjai, "Reproducibility of Turnover Rates in Heterogeneous Metal Catalysis: Compilation of Data and Guidelines for Data Analysis," Catal. Rev.-Sci. Eng. 39, 49-76 (1997).

2. CO Adsorption/Dissociation and Carbon Hydrogenation on Unsupported Iron Fischer-Tropsch catalysts

Hu Zou and Calvin H. Bartholomew
BYU Catalysis Lab, Department of Chemical Engineering
Brigham Young University, 350 CB, Provo, UT 84602, email: bartc@byu.edu

Significant previous work has focused on CO adsorption/dissociation over Fe FT catalysts for the purpose of better understanding the mechanism of Fischer-Tropsch Synthesis (FTS). The most widely-accepted FTS mechanism is the carbene model, involving CO adsorption and dissociation to adsorbed C and O atoms, hydrogenation of C atoms to CH_x species, and insertion of CH_x monomers into the metal-carbon bond of an adsorbed alkyl chain. Nevertheless, further quantitative study of CO adsorption and dissociation and of carbon hydrogenation on Fe surfaces is needed for the development of microkinetic models for FTS.

Unsupported Fe FT catalysts with/without K and/or Pt were prepared by a nonaqueous evaporative deposition method. Temperature programmed desorption (TPD) was used to study CO adsorption and dissociation. Isothermal hydrogenation and temperature programmed hydrogenation (TPH) were used to measure rates of hydrogenation of the carbonaceous adsorbed species after CO/H_2 treatment. Experiments were carried out at different CO adsorption temperatures. Two desorption peaks, associated with molecularly-adsorbed CO and dissociated CO respectively, were typically observed in CO-TPD spectra. Rates of desorption decreased for dissociated CO with increasing adsorption temperature. Quantitative analysis of the data is expected to provide information about the heat of adsorption and the kinetics of carbon hydrogenation on polycrystalline Fe.

3. CO Adsorption/Dissociation and Carbon Hydrogenation on Iron Fischer-Tropsch Catalysts

Hu Zou, Uchenna Paul, and Calvin H. Bartholomew
BYU Catalysis Lab, Department of Chemical Engineering
Brigham Young University, 350 CB, Provo, UT 84602, email: bartc@byu.edu

Significant previous work has focused on CO adsorption/dissociation over Fe FT catalysts for the purpose of better understanding the mechanism of Fischer-Tropsch Synthesis (FTS). The most widely-accepted FTS mechanism is the carbene model, involving CO adsorption and dissociation to adsorbed C and O atoms, hydrogenation of C atoms to CH_x species, and insertion of CH_x monomers into the metal-carbon bond of an adsorbed alkyl chain. Nevertheless, further quantitative study of CO adsorption and dissociation and of carbon hydrogenation on Fe surfaces is needed for the development of microkinetic models for FTS.

Unsupported Fe FT catalysts with/without K and/or Pt were prepared by a nonaqueous evaporative deposition method. Temperature programmed desorption (TPD) was used to study CO adsorption and dissociation. Isothermal hydrogenation and temperature programmed hydrogenation (TPH) were used to measure rates of hydrogenation of the carbonaceous adsorbed species after CO/H_2 treatment. Experiments were carried out at different CO adsorption temperatures. Two desorption peaks, associated with molecularly-adsorbed CO and dissociated CO respectively, were typically observed in CO-TPD spectra. Rates of desorption decreased for dissociated CO with increasing adsorption temperature. Quantitative analysis of the data is expected to provide information about the heat of adsorption and the kinetics of carbon hydrogenation on polycrystalline Fe.

4. A Theoretical Comparative Study of Fischer-Tropsch Synthesis on Fe and Co Surfaces

Rahul Nabar, Amit A. Gokhale, and Manos Mavrikakis
Department of Chemical Engineering, University of Wisconsin - Madison, 1415 Engineering Dr., Madison, WI 53706. email: manos@engr.wisc.edu

Fischer-Tropsch synthesis represents an industrially important catalytic reaction for the formation of higher hydrocarbons, starting from synthesis gas (CO and H_2). A periodic, self-consistent, Density Functional Theory analysis of the elementary steps up to C_2 hydrogenation on pure Fe(110), subsurface-carbon modified Fe(110), and Pt-modified Fe(110) surfaces will be presented and contrasted to the corresponding elementary steps on Cobalt surfaces.